Lab on a Chip

Accepted Manuscript

ROYAL SOCIETY OF CHEMISTRY

www.rsc.org/loc

Journal Name

RSCPublishing

ARTICLE

A medium throughput device to study the effects of combinations of surface strains and fluid-flow shear stresses on cells

Cite this: DOI: 10.1039/x0xx00000x

Received 00th January 2012,
Accepted 00th January 2012

DOI: 10.1039/x0xx00000x

www.rsc.org/

R. Sinha,[a] S. Le Gac,[b] N. Verdonschot,[a] A. van den Berg,[b] B. Koopman[a] and J. Rouwkema[*a]

We report a medium throughput device to study the effects of combinations of two mechanical stimuli – surface strains and fluid flow shear stresses, on cells. The first generation prototype can screen combinations of five strain and five shear stress levels. Computational modeling and empirical measurements were used to determine the generated strains and flows. Uniform equibiaxial strains up to 20% and shear stresses up to 0.3 Pa can be generated. Compatibility of the device with cell culture and end point fixation, staining and imaging is shown using C2C12 mouse myoblast cells.

Introduction

It is well known that cells sense and respond to local mechanical signals and geometry.[1] These physical factors can influence cell behaviors such as differentiation, proliferation, alignment and apoptosis.[1] Hence the physical factors are of great significance for tissue engineering and regenerative medicine, where often the goal is to control local tissue development. Physical factors are especially relevant for the development of complex, multi-cellular tissues, such as a pre-vascularized tissue. In such tissue, chemical factors, which are difficult to localize, are not optimal for controlling the development of all tissue components. Pre-vascularized tissue development is a promising strategy to overcome a nutrition-diffusion based size limit on engineered tissue.[2] The successful integration of a pre-vascular network has been shown amongst others for engineered muscle[3] and bone[4] tissues but the integration of this pre-vascular network with the in-vivo vasculature following implantation is not always optimal in the case of pre-vascularized bone. Since both bone and blood vessel formation in-vitro are known to be improved by mechanical stimulation,[5, 6] we wish to investigate the effect of mechanical stimulation on pre-vascularized bone development and improve models predicting tissue formation in scaffolds based on local mechanical stimuli.[7]

Mechanical signals can be applied to cells through resistance to their internal forces (for example substrate stiffness) or in the form of external mechanical stimuli (for example substrate strain, fluid flow shear stress, hydrostatic pressure). However, in order to use these signals to control cellular behavior, we first need to know in detail how cells actually respond to such signals. The effects of two mechanical stimuli - substrate strains and fluid flow shear stresses have been widely studied for a variety of cell types.[8] These mechanical stimuli are commonly present in the body, for example in blood vessels, lungs, heart and gut; and they can be applied to cells in a controlled way in the lab. Cell response is influenced by variations in these stimuli, such as in the magnitude, frequency and duration of stimulus application.[9, 10] Therefore, many experiments are required to find the optimum conditions for the cells. Therefore, high throughput techniques have been developed to study several conditions simultaneously. High throughput platforms have been reported that look at multiple fluid flow shear stresses[11, 12] and others that look at multiple substrate strains.[13-15] Since in-vivo the two mechanical stimuli are present simultaneously, the effects of a combination of the two stimuli have also been studied,[16-19] but the reported systems can look at only a single combination or at most a few combinations of the two stimuli at a time. In this paper, we report a platform to increase the throughput for studying the effects of combinations of substrate strains and fluid flow shear stresses.

A device has been developed to look at the effects on cells of combinations of five substrate strains and five fluid flow shear stresses, each with four replicates (giving a total of 100 units). Each unit has a region where a combination of a uniform equibiaxial surface strain and a fluid flow shear stress can be applied to cells. The generation of the various equibiaxial strains as well as the various flow regions has been shown in computational models and verified empirically. Furthermore, the variations in the fluid flow (and hence the generated shear stresses) caused by the strain actuation mechanism have been minimized. Compatibility of the device with cell culture and fluorescence microscopy to quantify cellular responses has been shown using C2C12 cells.

Materials and Methods

Device design and fabrication

The device (fig. 1) consists of an array of strain units producing a variety of strains, overlaid with a varying width fluid flow channel producing a variety of shear stresses. Strain in a unit is

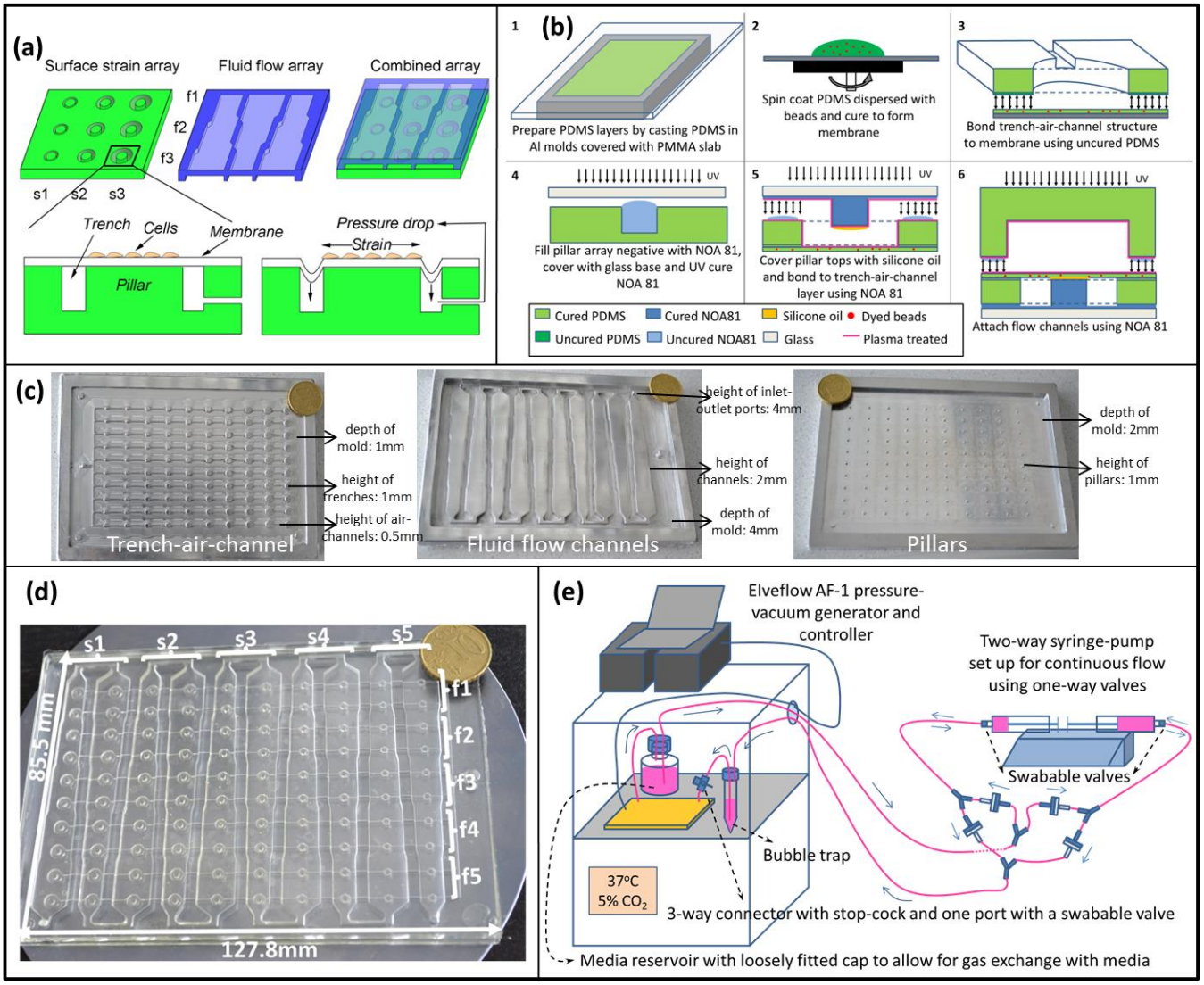

Fig. 1 The device schematic (a) shows the device design and the mechanism of strain generation. The device is fabricated in layers made by casting PDMS in aluminum molds (c). The device assembly is shown schematically for a single unit (b, steps numbered corresponding to description in the main text) and a finished prototype is shown (d). The various strain regions (s1, s2, s3…) and the various flow regions (f1, f2, f3…) are marked on the schematic and the prototype. For cell studies, the device is operated while stored inside a 37°C, 5%CO_2 incubator and connected to two pumps, one controlling the strain actuation air pressure and another controlling the fluid flow (e).

produced by deforming a thin flexible membrane over a stiff cylindrical pillar using a pressure drop, and is varied between units by varying the size of the pressure actuation cavity (hereafter referred to as the trench) around the pillar. The trenches are connected to the pressure source and to each other by air-channels so that the pressure drop can be driven from a single point.

The device assembly steps, shown schematically in fig. 1(b), were as follows: (1) The device layers were fabricated using a casting of polydimethylsiloxane (PDMS) (Sylgard 184, 10:1 base:curing agent ratio) in molds. Three molds (fig. 1(c)) were prepared by milling aluminum blocks: (i) a pillar array to generate a PDMS negative for pillars; (ii) a mold for a trench-air-channel layer; and (iii) a mold for fluid flow channels. After filling with PDMS, the molds were covered with a polymethylmethacrylate (PMMA) slab to acquire a flat surface. (2) A PDMS membrane was prepared by spin coating PDMS containing dyed polystyrene beads (6 µm, red, Polysciences Inc.), on an 8-inch silicon wafer (Siegert Wafer GmbH) rendered non-stick by a vapor deposited perfluorodecyltrichlorosilane (FDTS) coating. The spinning program used ran for 5 seconds at 100 rpm followed by 40 seconds at 1000 rpm. (3) The trench-air-channel layer was bonded on the side without the air-channels to the PDMS membrane using uncured PDMS as glue. The glue application was achieved by spin coating (2000 rpm for 2 minutes) a thin layer of PDMS on a silicon wafer and stamping it on the trench-air-channel layer. (4) A pillar array made using a NOA81 (UV curable glue, Norland Products Inc.) casting into the PDMS pillar array negative,[20] was assembled on a borosilicate glass base. (5) The tops of the pillars were covered with silicone oil (Griffon HR260 siliconespray) lubricant by manually placing drops of the lubricant and then the trench-air-channel layer was attached on the air-channel side to the pillar array using NOA81 as glue. The glue was applied to the trench-air-channel layer by placing drops of glue and manually spreading. To prevent glue

from entering the trenches and the air-channels, a physical blocking unit was prepared by filling the cavity formed by these features with NOA81 and curing it. The blocking unit was placed in the cavity during glue application and removed later. Both surfaces were plasma treated before binding using NOA81 to achieve a stronger bond. (6) Finally the fluid flow channel structure was bonded on top using NOA81 as glue. The glue was applied to the fluid flow channel layer by placing drops and manually spreading. In this step too, both surfaces were plasma treated before binding using NOA81 to achieve a stronger bond. PDMS was always cured at room temperature for 48 hours (except for the membrane, which was cured at 60^{o}C for ~2 hours) to avoid mismatched shrinkages in the various layers.

The key dimensions of the device are: radius of pillars 0.75 mm; height of pillars 1 mm; distance between pillar centers 7mm (along device width) and 11mm (along device length); trench-air-channel layer thickness 1 mm; trench height 1 mm; air channel height 0.5 mm; air channel width 0.5 mm; trench radii – 1 mm, 1.25 mm, 1.5 mm, 1.75 mm and 2 mm; fluid flow channel height 2 mm; fluid flow channel regions' widths 6 mm, 7 mm, 8 mm, 9 mm and 10 mm; membrane thickness 80 µm. The membrane thickness was measured by imaging the cross-section of a small strip of the membrane, while the other dimensions were treated as accurate within the precision limit of the milling machine.

Computational Modeling

Computational models were developed using ANSYS 13.0 Workbench (ANSYS Inc.) to simulate the operation of the device. Three models were developed : a single strain unit, the complete fluid flow channel and a single unit with combined strain and fluid flow.

For the strain unit model, a quarter of the unit was modeled under symmetry conditions. The PDMS parts were modeled as flexible bodies with an elastic modulus of 1.84 MPa[21] and the pillar was modeled as a rigid body (since NOA81 is much stiffer than PDMS and unlikely to deform under the applied conditions). PDMS-PDMS contact was modeled as bonded and PDMS-pillar contact as frictional. A coefficient of friction of 0.01 was used between pillar and PDMS, based on a pin-on-disk (NOA81 pin, PDMS disk) experiment with silicone oil lubrication (data not shown). The base of the unit was constrained as fixed and a linearly increasing pressure drop was applied to the bottom surface of the PDMS membrane. The strains generated on the top surface of the membrane were analyzed.

The fluid flow channel geometry was drawn in SolidWorks (Dassault Systemes) and the model was solved using ANSYS FLUENT (ANSYS Inc.). A simple laminar flow model was used with a velocity inlet and a pressure outlet. The effects of changing flow velocity, fluid viscosity and channel height on the wall shear stress were analyzed.

The effect of strain actuation on fluid flow generated wall shear stress was analyzed by means of a two-way fluid structure interaction (FSI) analysis of a device unit with both strain and fluid flow. The variation of wall shear stress was monitored over a strain cycle both with and without fluid flow and the same was repeated for a lower height flow channel of 0.5 mm. A 1 second cycle was modeled at a constant fluid flow and a linearly varying pressure drop varying between 0 and 40 kPa (fig 2(f)). For the conditions under which flow was present, the model was solved for two cycles, so as to include the dynamics of the system at the start of a cycle.

To isolate the contribution of the geometry change during strain actuation on the fluid flow, the flow was modeled for several fixed geometries with the membrane in various deformed states. The deformation of the membrane was modeled as a circular arc with various maximum dips from the surface.

A 20 ml/min volumetric flow rate, 0.001 Pa-s viscosity (viscosity of water at 20^{o}C), 1000 kg/m^{3} density (density of water) and 2 mm channel height were used for the fluid dynamics models, except when studying the effects of variations in those parameters. The 20 ml/min volumetric flow rate translated to a 0.1 m/sec inlet velocity for the complete fluid channel array (2 mm diameter circular inlet) and a 0.03 m/sec inlet velocity for the section used for the FSI analysis (6 mm x 2 mm rectangular inlet), both values rounded to one significant figure.

Device characterization

The strain array and the fluid flow channels were characterized by tracking 6 µm beads (red, Polysciences Inc.) embedded in a membrane and suspended in fluid respectively.

A strain array was assembled and actuated using an Elveflow® AF1 dual pressure-vacuum generator and controller combination (Elvesys® Innovation Center). For strain measurements, images were taken at various stretch positions, the bead co-ordinates were extracted, the center of deformation was approximated and radial strains were determined from them. Bead co-ordinates were extracted using a maxima/minima finding command in ImageJ (NIH). To eliminate points incorrectly identified as beads and to map bead positions in images for various strains, a custom-written MATLAB® (MathWorks Inc.) script was used that checked that a bead and its two nearest neighbors were present in all images, displaced and changed in relative orientation within specified limits. Centre approximation and strain calculations were also done using custom MATLAB® (MathWorks Inc.) scripts.

As has been noted previously,[13] a setup like this is unsuitable for circumferential strain measurements. Moraes et.al. used an arbitrary reference line and measured circumferential movements with respect to that line, and found that this method of circumferential strain determination was not sufficiently robust due to sensitivity to errors in center determination as well as errors in the location of the reference line (measurements close to the arbitrary line were less accurate). Therefore, to show the equibiaxial nature of the strain, we calculated the linear strains between pairs of beads and plotted them against the angle between the line connecting the beads and the horizontal direction in the images (orientation

angle of bead pair). This will result in the same strain values for all orientation angles for a perfect equibiaxial system.

The strain measurements were performed for all 100 units (n=20 per strain condition). Also, strains of five units were determined at various intervals after continuous use to see variations in generated strains over a long duration of use.

For fluid flow measurements, fluid flow channels were attached to a PDMS-coated glass base and water with suspended beads (6 µm, red, Polysciences Inc.) was flown through them using a syringe pump. Fluid velocities in the various flow regions were measured by tracking the beads. 10 beads were tracked for each region to get an average velocity. Images were taken in the centers of the five flow regions in a plane at approximately half the channel height. Bead tracking and flow velocity calculations were done from these images using the ImageJ (NIH) manual tracking plugin.

Screening for the effect of mechanical stimulation on C2C12 cells

Cell Culture To validate the compatibility of the device with cell culture and to investigate the response of cells to various mechanical stimuli, cells were seeded on devices coated with fibronectin (Sigma-Aldrich F1141).

The flow channels were assembled just before the cell experiments so that the plasma treatment and the UV treatment involved in this step sterilized the device for cell culture. The flow channels, right after assembly, were filled with a 0.5µg/ml fibronectin solution and incubated for ~1 hour at room temperature. ~10,000 C2C12 cells/cm^2 in C2C12 medium: Dulbecco's Modified Eagle's Medium(DMEM; Invitrogen) supplemented with 10% FBS(Invitrogen), 1% penicillin and streptomycin (Invitrogen), 1% L-glutamin (Invitrogen) & 0.1% fungizone (Invitrogen), were seeded in the device directly after removing the fibronectin solution. While filling an empty device with fluid, it was tilted so that the fluid front moved ahead against gravity. This prevented any bubbles from being trapped as the bubbles rose against gravity and went to the fluid front and were finally pushed out of the device.

After cell seeding, the device was incubated in a 37^{o}C, 5% CO_2 incubator. The cells were allowed to attach and grow under static conditions for 18 hours and then mechanical stimulation was applied for 6 hours. Three mechanical stimulation conditions were applied on separate devices – flow only, strain only and flow-strain combination. 20ml/min flow (~0.07-0.13 Pa shear stress range) and a sinusoidal pressure cycle with 0-400mbar (pressure drop) range and 1 second period (~2-20% strain range) were applied. Cells were also cultured on another device for 24 hours without any mechanical stimulation as a control. The pumps for applying the flow and the strains were stored outside the incubator and connected to the device through a side hole (fig. 1(e)). A two-way syringe pump was set up for applying continuous flow using one way check valves (Value Plastics). The syringes filled from and emptied (after flowing through the device) into a common reservoir (100ml flask, Elvesys). The flow entered the device through a bubble trap (10ml tube). A three-way connector with a stop-cock and one port with a swabable valve was used at the device inlet, which allowed for cell seeding without opening the flow circuit.

The experiments were stopped at 24 hours and the cells were fixed with 4% paraformaldehyde for 10 minutes and stored under PBS at 4^{o}C. Fixed cells were stained with Phalloidin (Alexa Fluor 488) and DAPI after permeabilization with 1% Triton X-100 and blocking with 5% bovine serum albumin (BSA). After staining, the PDMS over the flow channels was removed to allow for better microscopy access.

Imaging and Data Analysis Imaging was done using BD Pathway with a 4x objective which captured a frame of size 2.1mmx1.6mm. A macro was used to focus and capture images throughout the device in an automated fashion. Images were captured over each pillar (area over a pillar hereafter referred to as region of interest (ROI)) and the unstrained region between each pair of ROIs along the flow channel. The images were corrected for non-uniform illumination by applying a 10 pixel rolling ball radius background subtraction using ImageJ. For ROI images, the area outside the circular ROIs in the rectangular images were cleared by manual selection, also using ImageJ. The images thus processed were analyzed using a CellProfiler[22] pipeline – the nuclei were identified as primary objects (adaptive background thresholding and intensity based separation of clumped objects were used) from the DAPI images, the cells were identified from the phalloidin images as secondary objects around the nuclei (using the Distance-B method on phalloidin images with adaptive background thresholding) and shape and size parameters were measured for both. Orientation of cells measured by CellProfiler was converted to radial/circumferential orientation with respect to the ROI centers (angle between cell fit ellipse major axis and line joining cell center and ROI center) using a custom MATLAB script. The data was averaged per image (ROI or region between ROIs) and then the ROI averages were grouped by condition (strain, flow, strain-flow combination) and analysis of variance was performed using MATLAB functions (anova1 or anova2 depending on whether the effects of one or two conditions were considered). Also, all ROI averages and all regions between ROI averages were grouped and compared using a T-test (MATLAB ttest2 function).

Results

Computational Modeling

Analysis of the strain unit showed that uniform equibiaxial strains can be generated at the top surface of the membrane over the pillar. The strain is higher at a higher pressure drop, and at a given pressure drop a higher radius trench can generate a higher strain. The radial strain generated is uniform over the central region above the pillar and increases near the edge. The

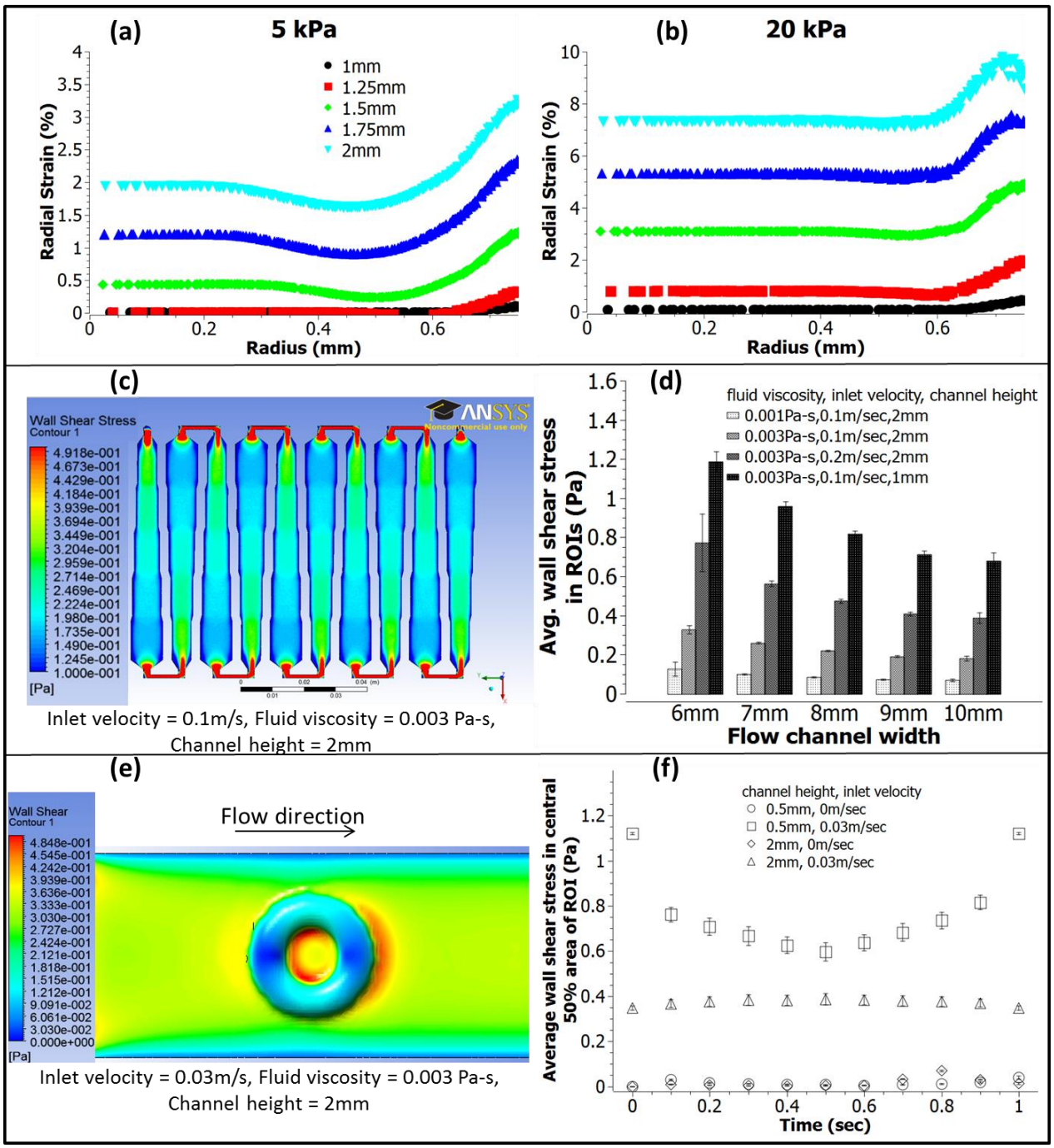

Fig. 2 Computational modeling was done using ANSYS. The strain generation was modeled for a quarter strain unit with symmetry boundary conditions and showed the generation of uniform strain regions in the ROIs. The uniform strain regions became bigger with increasing pressure drop as shown in the radial strain vs. radius plots at 5 kPa (a) and 20 kPa (b). Fluid flow was modeled for the complete flow channel setup (c) and showed the generation of the various shear stress regions. The shear stresses generated can be varied by changing the fluid viscosity, flow rate or channel height (d). A fluid structure interaction (FSI) model was used to study the effects of the strain actuation mechanism on the fluid flow shear stress in the ROI (e) and showed that using a high channel reduces the effect (f). The results shown are for the 2nd cycle for the conditions under which flow was present.

region of uniform strain becomes bigger with increasing pressure – at 5kPa a central region of radius ~0.3mm has a uniform strain (fig. 2(a)) while at 20kPa the uniform strain region spreads to a ~0.6mm radius (fig. 2(b)).

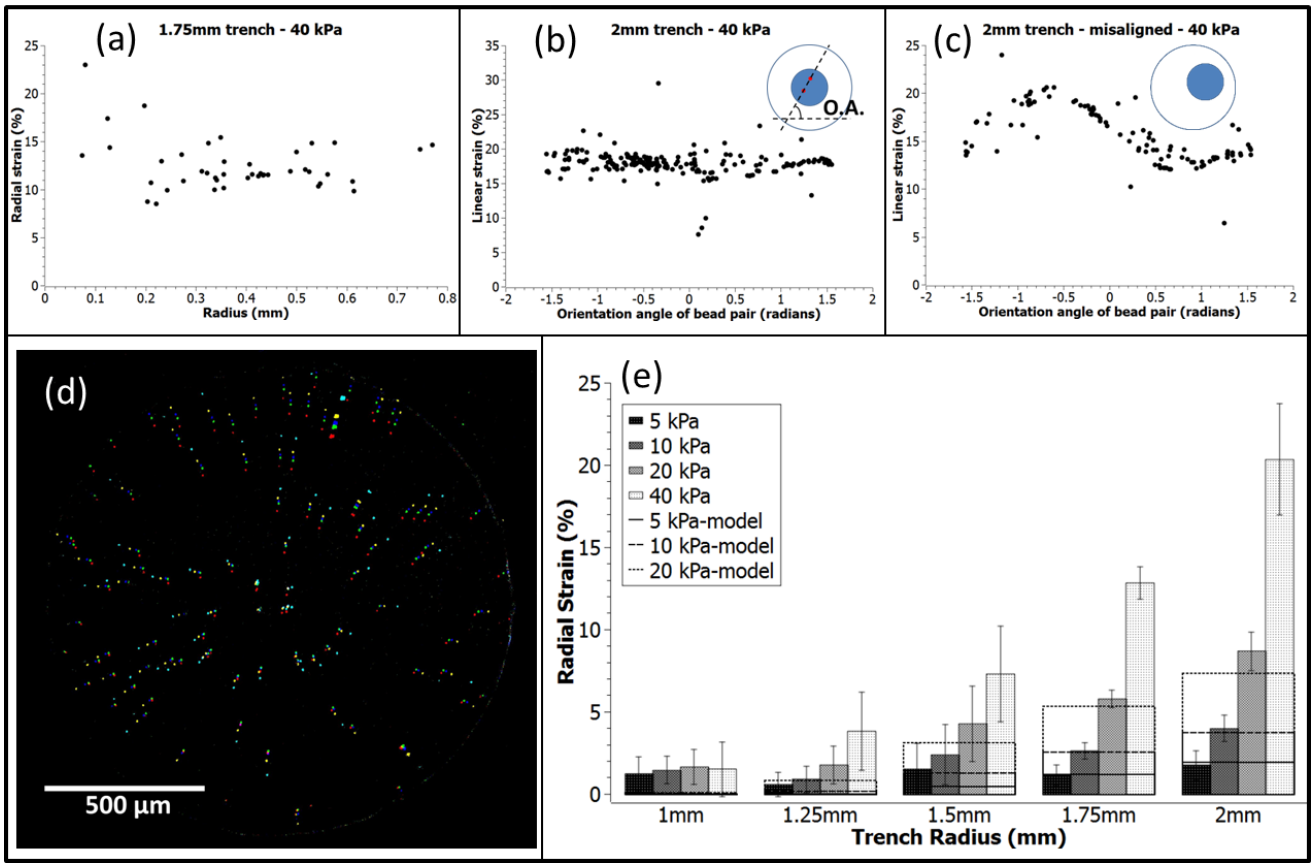

Fig. 3 Strains were empirically determined by tracking beads embedded in the stretching membrane in images taken at varying strains. A customized program was used to extract bead co-ordinates in images and identify beads that were detected in all images. Center of deformation was determined from the bead paths as well as visually approximated from an overlay of bead positions at varying strains (d). Radial strains were then calculated and plotted against radius (a). The linear strain between each pair of detected beads is plotted against the orientation angle (O.A.) of the beads to check if the generated strains are equibiaxial (b) or have directional variations (c) due to fabrication effects such as misalignment. The average radial strains determined empirically for all units at multiple pressure drops were averaged for all the units with the same trench size (n=20 per trench size; standard deviations shown as error bars) and compared with model-determined values (e).

Analysis of the fluid flow showed the generation of various shear stress regions corresponding to the various channel widths (fig. 2(c)). Fig. 2(d) shows - for each flow region - the average shear stress in the ROIs. The large standard deviation error bars for the 6mm and 10mm regions are caused by these regions lying next to bends and areas of sudden large dimension change, which were allowed in the design due to geometric constraints. This effect can be minimized by increasing the fluid viscosity, as shown by the smaller error bars. Increasing the viscosity has the added advantage of increasing the shear stress. Higher shear stresses can also be achieved by using a higher flow rate, but this will increase the effects of the bending and the sudden dimension change as was shown by a doubling of the flow rate (fig. 2(d)). An additional method to achieve higher shear stresses without increasing the bending and sudden dimensional change effects is to use a lower height flow channel (fig. 2(d)).

Fluid structure interaction (FSI) analysis enabled visualization of the changes in the flow and the generated shear stress due to the strain-producing membrane deformation. In the case of a 2mm high channel and a ~20ml/min flow rate (0.03m/sec inlet velocity), there was an increase in the average shear stress in the ROI during the strain cycle, while in the case of a 0.5mm high channel with the same inlet velocity the average shear stress in the ROI decreased during the strain cycle. The variations in the average shear stress in the ROI over a strain cycle were higher for the 0.5mm channel (maximum 40% decrease from initial value for the 0.5mm channel and maximum 17% increase from the initial value for the 2mm channel). The shear stress distribution variability in the ROI was also higher for the 0.5mm channel (maximum standard deviation to average value ratio 0.11 for 2mm channel and 0.17 for 0.5mm channel). The shear stress variations were higher at the ROI edge and choosing a smaller ROI (the central 50% area of the original ROI) reduced the shear stress distribution variability (maximum standard deviation to average value ratio 0.06 for 2mm channel and 0.07 for 0.5mm channel). For the smaller ROI the variation in average shear stress over a strain

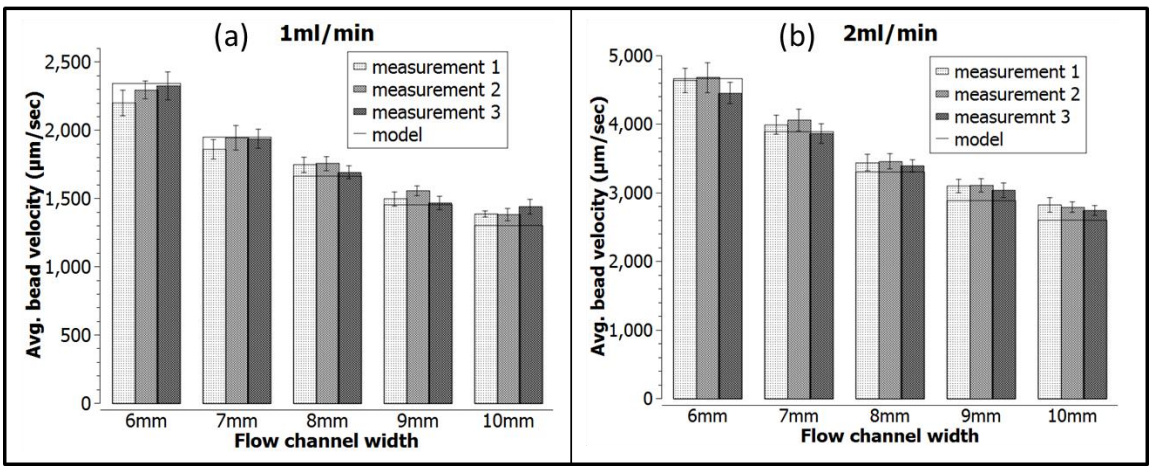

Fig. 4 Flow velocities were measured in the center of each flow region at half channel height by tracking suspended beads. Three measurements were taken in each region and for two flow rates, namely1ml/min (a) and 2ml/min (b). Flow velocities in both cases showed good agreement with values determined by modeling .

cycle was lower than the original ROI for the 2mm channel and higher than the original ROI for the 0.5mm channel (maximum 47% decrease from initial value for the 0.5mm channel and maximum 11% increase from the initial value for the 2mm channel). FSI analysis under the stationary fluid conditions showed shear stresses an order of magnitude smaller than the shear stresses generated under the applied flow conditions for both channel heights used.

The fluid flow models with the fixed geometries showed a ROI shear stress variation in response to increasing membrane deformation, which is very similar to that observed in the FSI analysis (Supplementary fig. 1). This demonstrates that the membrane motion is slow enough for the flow to be primarily determined by the local channel geometry. Thus at this device operation frequency, the fixed geometry models provide a computationally easier way to investigate the device behavior.

Device characterization

The membrane thickness was found to be 80.9±3.9 µm based on single measurements on 25 membranes.

Radial strains determined by tracking embedded beads were plotted against radii for all 100 strain units on a device. For each unit, over 100 points were identified as beads initially. After the mapping between the image sets, on average 18 beads were detected and used to determine the strains. No centering was applied for bead detection, which gives a maximum possible error equal to the bead radius (3µm, which corresponds to 5 pixels in the images used) in the detection of the bead co-ordinates. Fig. 3(a) shows a typical plot with a higher spread in the strain near the smaller radii, possibly due to the errors in bead location and center determination being comparable to the distances determined from them. The plots of the strains between pairs of beads against the bead pair orientation typically showed that the strains were the same in all directions (equibiaxial strain, fig. 3(b)). The bead pairs for which the beads were close together were generally responsible for the very low or very high strain values, an effect similar to the strains for small radii, explainable by the errors and distances being similar in magnitude. Misalignment of pillars with respect to the trenches was sometimes observed, which led to the centers of deformation not coinciding with the pillar centers. Due to this, anisotropies in the biaxial strain were observed (fig. 3(c)). The effects of the misalignment on the strains generated and the equibiaxial nature of the strains generated were more prominent in the case of the small trench sizes.

When grouped by trench size, the averages of the average radial strains for each unit showed the expected pattern, namely increasing radial strain with increasing trench size. The results compared well with those of the computational models, except for the two smallest trench sizes. However this difference could be explained by the increased sensitivity of the strain measurements to misalignments in those cases, since small misalignments brought the pillar to one corner of the trench.

Strain measurements after continuous cyclic straining at 1 Hz showed a decrease in the strains to 80% of initial strains after 24 hours of operation. The results were similar when testing in air at room temperature or under cell culture media at 37^{o}C. The lubricant layer showed thinning after the 24 hour testing but did not show any signs of evaporation, and strains generated were similar before and after a ~4 month storage period.

Fluid velocity measurements by bead tracking showed good agreement with the predicted fluid flows of the computational models (fig. 4).

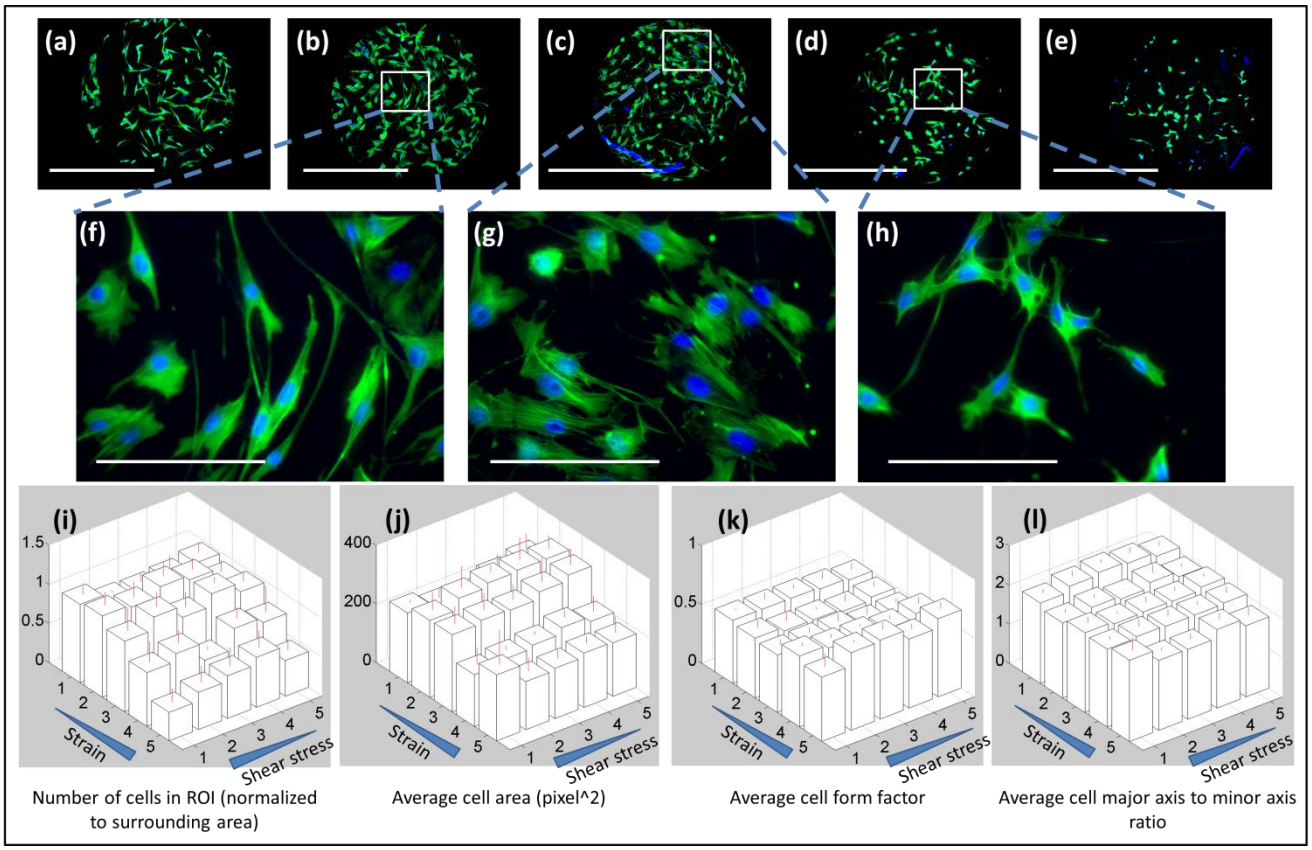

Fig. 5 Screening for the effects of mechanical stimulation was performed for C2C12 cells. Cells were cultured on the device statically for 18 hours and then stimulated with flow only, strain only, or flow-strain combination for 6 hours. Cells were then fixed with paraformaldehyde and stained for filamentous actin (phalloidin, green) and cell nuclei (DAPI, blue). Significant differences were observed between the cells subjected to the various strains (a:1.5%, b:4%, c:7%, d:13% and e:20% strain, scale bar 1mm) but no significant differences were observed between the various flows. The system is compatible with higher magnification imaging, which makes it fit for the screening of intracellular responses (f-h, scale bar 200µm). Cell and nuclei images were segmented and measured using CellProfiler. Measured cell shape and size descriptors were grouped by condition and compared (i-l, mean values are depicted including standard deviations (n=4)).

Screening for the effect of mechanical stimulation on C2C12 cells

Cells remained attached and exhibited a spread out morphology for the experiment duration of 24 hours, indicating that cells remained viable on all tested devices. Imaging was shown to be possible with a 4x objective having the whole ROI in a frame as well as using a 20x long working distance objective for capturing more details, for example actin stress fibers. Images could be segmented to detect the cells and the nuclei and measure various shape and size descriptors. C2C12 cells showed significant overlap, as has also been observed previously,[15] making segmentation harder and cell shape/size descriptors less reliable. As examples, averages of measured cell area, cell form factor(4πArea/Perimeter^2) and cell major axis to minor axis ratio are shown for the 25 conditions on the device subjected to combined flow-strain stimulation (fig. 5(g)-(j)). Statistical analysis was performed on this data (supplementary table 1). For the C2C12 cells under the applied mechanical stimuli, differences were observed between the various strain conditions but not the various flow conditions. Regions exposed to higher strains showed fewer, smaller and more rounded cells. C2C12 cells are known to align perpendicular to uniaxial strains, but no specific alignment was observed in response to strains in our experiments. This could be expected since the strains were equibiaxial and it has been previously observed that C2C12 do not align when exposed to equibiaxial strains.[14] Cell alignment was also not observed in response to flow, which could be a cell specific result or because of the shear stress magnitude and duration not being high enough to elicit an alignment response.

Discussion

Mechanical stimuli are important for tissue engineering approaches. In particular, they offer an important method of controlling tissue development for complex, multi-cellular tissues, where other approaches such as chemical factors encounter localization problems. However, in order to use mechanical signals to control tissue development, researchers

must know in detail how cells respond to single and combinations of mechanical signals. Also, a quantitative optimization of the mechanical stimuli is needed for tissue engineering. The reported device is a tool developed to enable this optimization with increased efficiency by using a high throughput approach. Even though devices have been previously developed to study the effect of surface strains,[13, 14] or fluid shear stresses[11, 12] in high throughput, or the combination of the two stimuli with multiple strain conditions but a single fluid flow shear stress condition,[23] to our knowledge, this is the first reported device to study combinations of multiple substrate strains and multiple fluid flow shear stresses in high throughput.

A design requirement that was set for this device was having the ROIs big enough to study a few hundred cells, so that co-cultures of cells could be studied. Millimeter scale features were therefore chosen. While this had a few disadvantages in comparison to smaller microfabricated features, such as the need for large cell numbers and a requirement for more culture media, there were also some advantages. One advantage of working with this feature size is that the molds for casting device parts can be easily made using an automated milling machine as compared to the complex mask making and lithography setups required to make microfluidic molds. Also, features of different heights can be made relatively easily, which in microfabrication would need to be done in separate layers demanding fine alignment. Also, the height of features that can be made using the commonly used microfabrication technique of making SU-8 molds is limited by the depth of SU-8 that can be UV-cured.

The device's external dimensions are the same as a standard 96-well plate, allowing for ease of imaging using a bio-imager such as the BD Pathway™ (BD Biosciences). The transparency of the device allows imaging using inverted as well as upright microscopes. The pillars are all of the same size so that the surface area covered with cells and exposed to the mechanical stimuli is the same for all the units, allowing for a better comparison. For simplicity, all strain units are connected to a single opening for pressure control and there is a single pair of inlet and outlet points for fluid flow. A common fluid flow between units was chosen under the assumption that any paracrine signaling will be washed away by the continuously flowing media.

The pressure drop based strain actuation, besides its self-evident advantages of producing planar uniform equibiaxial surface strains and keeping the cells in a plane allowing for real-time imaging, has an additional advantage over pressure increase based strain actuation,[24, 25] which is that there is a lower risk of device layers delaminating.

Estimating the effect of the strain generating mechanism on the fluid flow and minimizing it was an important part of the device design. From parallel plate fluid flow chamber studies it is well known that fluid flow shear stress depends on the flow rate, fluid viscosity and channel dimensions ($\tau=6Q\mu/(wh^2)$, where τ is the shear stress, Q is the flow rate, μ is the dynamic viscosity, w is the width of the channel and h is the channel height). The expected cause of disturbance in the shear stresses experienced by the cells placed in the ROIs in the device was the flow initiated by the fluid displaced during the strain actuation. A higher flow rate compared to these disturbed flows would therefore mask their effects. However the high flow rates would increase the shear stresses generated, an effect which could be compensated for by increasing the channel height. This simplistic analysis was used to help choose the channel height for the device. The FSI analysis further served as a useful tool to estimate the shear stresses generated and the variations caused by the strain actuation for the actual device geometry, which was more complex than for the parallel plate flow chambers. The directional fluid flow made it hard to find any symmetric conditions to reduce the size and complexity of the FSI computational model, as Brown et al[26] were able to do. Therefore only the area having the highest impact of strain actuation on fluid flow was chosen for the FSI analysis. The FSI analysis was done for the region with the biggest trench and the smallest fluid flow channel region. This region had the biggest membrane motion and the lowest total volume of fluid, making the displaced fluid volume to total fluid volume ratio the highest. The FSI analysis showed that a 2mm high channel gives a less disturbed flow than a 0.5mm channel (measured in terms of variation of mean shear stress in ROI over a strain cycle and the variability in distribution of shear stress in ROI at any given point). Despite the reduction in shear stress variation by increasing the channel height, this variation cannot be completely eliminated. At any given point, the variability in shear stress in the ROI is primarily near the edges and selecting a smaller area in the center of the current ROI as the new ROI can reduce this shear variability. The shear stress variations over a cycle are small for the high channel and comparable with effects of pulsatile flow shear stresses on the cells of interest, but must still not be ignored.

For device strain characterization, embedded beads were tracked. Previously, similar studies have made use of fluorescent beads deposited on the membrane[13] or a patterned membrane with small traceable features[14]. In both these approaches, the cells are likely to respond to these features. Since it is hard to wash off the beads or remove the features after measuring of the strains, the characterized strain membrane could not be used for the actual cell studies. Embedding beads in the membrane has the advantage of allowing the cell studies to be performed on the characterized membrane. To ensure that the bead embedding did not significantly change the mechanical properties of the membrane, the beads used were several times smaller than the membrane thickness (bead diameter 6 μm and membrane thickness 80 μm) and a low number of beads (total bead volume < 1/10000th of the total PDMS volume) were embedded. The low number of beads also ensures that they do not block imaging of cells later.

In the used configuration, the flow was switched between syringes (one syringe driving the flow while the other filled) every 1 minute. As per the manufacturer, the syringe pump switched direction in 0.25 seconds and during this time the built

up pressure in the bubble trap drove the flow. Hence the flow never stopped or switched direction, but only slowed down for ~1-2 seconds per minute.

Misalignment between device layers during assembly, the presence of bends and sudden dimensional changes in the fluid flow channel, and the drop in strains generated over long duration use are some limitations that will be addressed in designing the next-generation prototype. The strain variation over a long period of use is most likely due to thinning of the lubricant. Other similar systems have reported a lower variation in strains over long use[13, 14] when using different lubricants and so this will also be evaluated in future generation systems. Apart from that, pre-conditioning of the device may also stabilize the lubricant layer that remains and hence reduce further variations in the strains. The shear stresses generated in the current prototype are on the lower side of commonly tested ranges and hence the effects of higher shear stresses, which can be obtained by increasing the media viscosity (for example by addition of dextran[27]), will also be studied.

The developed system has been used to test the (combined) effect of surface strains and fluid flow shear stresses on C2C12 cells in order to demonstrate the applicability of the device. These experiments were successful in showing that differences in cell shape, cell size, and number of cells can be imaged and analyzed. It should be noted that the variance in the acquired data is relatively high. This is in part due to the overlap of the C2C12 cells, making segmentation harder and cell shape/size descriptors less reliable. Apart from that, cell shape and cell size are dependent on other factors that are not directly related to surface strains or fluid flow shear stresses, such as the proliferative state of cells, where cells that are in the process of division are often rounder and less spread.[28] By using fluorescent immunohistochemistry and focusing on output parameters that are directly influenced by mechanical signals, such as the presence and density of focal adhesion sites, it is likely that the output of the system can be enhanced, resulting in the improved distinction between cellular responses to different levels of mechanical stimulation.

As it has been shown that anisotropic strains can have different effects on cells compared to the equibiaxial strains such as those produced in the current device,[29] future generation prototypes will also include pillars of varying shapes to produce anisotropic strain profiles. The current device, operating at pressure drop as high as 40kPa, can generate strains in the range of 2-20% and with a 0.003 Pa-s viscosity fluid flowing at ~20ml/min can produce shear stresses in the range 0.18-0.33Pa. These ranges can be easily varied by operating the device under different conditions, namely a different strain range by changing the pressure drop and a different shear stress range by changing the flow rate. However as a starting point the two ranges provide relevant test conditions as cells have been shown to detect and respond to these levels of mechanical stimuli as well as showing variations within these ranges[11, 14].

Conclusions

A medium throughput device has been developed to study the effects of combinations of surface strains and fluid flow shear stresses on cells by using units that can be individually characterized. The fact that operation of the device does not have an effect on the plane where the cells are located makes this system highly promising for the real-time investigation of cellular behavior. The design considered the interaction of the two stimuli and attempted to minimize their impact on each other so that they could be independently varied. Straightforward fabrication and ease of use are strengths of the device. All in all, this provides us with an easily adaptable and flexible system to screen for the effects of mechanical signals on cells.

Acknowledgements

This work was supported by the Dutch Technology Foundation STW. We would like to thank Prof. Clemens van Blitterswijk and the group of Tissue Regeneration at the University of Twente for providing us with the reagents and the facilities for the cell studies, and Prof. Dik Schipper and Walter Lette at the Surface Technology and Tribology group at the University of Twente for their help with the friction coefficient measurement.

Notes and references

[a] Department of Biomechanical Engineering, MIRA Institute for Biomedical Technology and Technical Medicine, University of Twente, Enschede, The Netherlands.

[b] BIOS, Lab on a chip group, MIRA Institute for Biomedical Technology and Technical Medicine, MESA+ Institute for Nanotechnology, University of Twente, Enschede, The Netherlands.

Electronic Supplementary Information (ESI) available: [details of any supplementary information available should be included here]. See DOI: 10.1039/b000000x/

1. V. Vogel and M. Sheetz, *Nature Reviews Molecular Cell Biology*, 2006, **7**, 265-275.
2. J. Rouwkema, N. C. Rivron and C. A. van Blitterswijk, *Trends in Biotechnology*, 2008, **26**, 434-441.
3. S. Levenberg, J. Rouwkema, M. Macdonald, E. S. Garfein, D. S. Kohane, D. C. Darland, R. Marini, C. A. van Blitterswijk, R. C. Mulligan, P. A. D'Amore and R. Langer, *Nature Biotechnology*, 2005, **23**, 879-884.
4. J. Rouwkema, J. De Boer and C. A. Van Blitterswijk, *Tissue Engineering*, 2006, **12**, 2685-2693.
5. C. A. Simmons, S. Matlis, A. J. Thornton, S. Q. Chen, C. Y. Wang and D. J. Mooney, *Journal of Biomechanics*, 2003, **36**, 1087-1096.
6. T. Matsumoto, Y. C. Yung, C. Fischbach, H. J. Kong, R. Nakaoka and D. J. Mooney, *Tissue Engineering*, 2007, **13**, 207-217.
7. W. J. Hendrikson, C. A. van Blitterswijk, N. Verdonschot, L. Moroni and J. Rouwkema, *Biotechnology and Bioengineering*, 2014, **111**, 1864-1875.
8. T. D. Brown, *Journal of Biomechanics*, 2000, **33**, 3-14.
9. B. D. Riehl, J. H. Park, I. K. Kwon and J. Y. Lim, *Tissue Engineering Part B-Reviews*, 2012, **18**, 288-300.

10. K. T. Lim, H. Seonwoo, H. M. Son, S. J. Baik, J. H. Kim, S. H. Jeon, J. Y. Park, Y. H. Choung, C. S. Cho, P. H. Choung and J. H. Chung, *Tissue Engineering and Regenerative Medicine*, 2009, **6**, 1327-1342.
11. L. Wang, Z. L. Zhang, J. Wdzieczak-Bakala, D. W. Pang, J. M. Liu and Y. Chen, *Lab on a Chip*, 2011, **11**, 4235-4240.
12. L. Chau, M. Doran and J. Cooper-White, *Lab on a Chip*, 2009, **9**, 1897-1902.
13. C. Moraes, J. H. Chen, Y. Sun and C. A. Simmons, *Lab on a Chip*, 2010, **10**, 227-234.
14. C. S. Simmons, J. Y. Sim, P. Baechtold, A. Gonzalez, C. Chung, N. Borghi and B. L. Pruitt, *Journal of Micromechanics and Microengineering*, 2011, **21**.
15. Y. Kamotani, T. Bersano-Begey, N. Kato, Y. C. Tung, D. Huh, J. W. Song and S. Takayama, *Biomaterials*, 2008, **29**, 2646-2655.
16. H. J. Kim, D. Huh, G. Hamilton and D. E. Ingber, *Lab on a Chip*, 2012, **12**, 2165-2174.
17. D. Huh, B. D. Matthews, A. Mammoto, M. Montoya-Zavala, H. Y. Hsin and D. E. Ingber, *Science*, 2010, **328**, 1662-1668.
18. W. F. Zheng, B. Jiang, D. Wang, W. Zhang, Z. Wang and X. Y. Jiang, *Lab on a Chip*, 2012, **12**, 3441-3450.
19. M. Toda, K. Yamamoto, N. Shimizu, S. Obi, S. Kumagaya, T. Igarashi, A. Kamiya and J. Ando, *Journal of Biotechnology*, 2008, **133**, 239-244.
20. D. Bartolo, G. Degre, P. Nghe and V. Studer, *Lab on a Chip*, 2008, **8**, 274-279.
21. http://www.sandia.gov/polymer-properties/E1-Youngs_modulus.html.
22. A. E. Carpenter, T. R. Jones, M. R. Lamprecht, C. Clarke, I. H. Kang, O. Friman, D. A. Guertin, J. H. Chang, R. A. Lindquist, J. Moffat, P. Golland and D. M. Sabatini, *Genome Biology*, 2006, **7**, 30.
23. L. T. Breen, P. E. McHugh, B. A. McCormack, G. Muir, N. J. Quinlan, K. B. Heraty and B. P. Murphy, *Review of Scientific Instruments*, 2006, **77**.
24. K. Shimizu, A. Shunori, K. Morimoto, M. Hashida and S. Konishi, *Sensors and Actuators B-Chemical*, 2011, **156**, 486-493.
25. M. H. Wu, H. Y. Wang, H. L. Liu, S. S. Wang, Y. T. Liu, Y. M. Chen, S. W. Tsai and C. L. Lin, *Biomedical Microdevices*, 2011, **13**, 789-798.
26. T. D. Brown, M. Bottlang, D. R. Pedersen and A. J. Banes, *American Journal of the Medical Sciences*, 1998, **316**, 162-168.
27. V. I. Sikavitsas, G. N. Bancroft, H. L. Holtorf, J. A. Jansen and A. G. Mikos, *Proceedings of the National Academy of Sciences of the United States of America*, 2003, **100**, 14683-14688.
28. M. Thery and M. Bornens, *Current Opinion in Cell Biology*, 2006, **18**, 648-657.
29. J. S. Park, J. S. F. Chu, C. Cheng, F. Q. Chen, D. Chen and S. Li, *Biotechnology and Bioengineering*, 2004, **88**, 359-368.